APL Materials

Homoepitaxial β-Ga_2O_3 transparent conducting oxide with conductivity σ = 2323 S cm^{-1}

Cite as: APL Mater. **9**, 101105 (2021); https://doi.org/10.1063/5.0062056
Submitted: 01 July 2021 • Accepted: 14 September 2021 • Published Online: 12 October 2021

Hyung Min Jeon, Kevin D. Leedy, David C. Look, et al.

Homoepitaxial β-Ga_2O_3 transparent conducting oxide with conductivity σ = 2323 S cm^{-1}

Cite as: APL Mater. 9, 101105 (2021); doi: 10.1063/5.0062056
Submitted: 1 July 2021 • Accepted: 14 September 2021 •
Published Online: 15 October 2021

Hyung Min Jeon,[1,a] Kevin D. Leedy,[1] David C. Look,[1,2] Celesta S. Chang,[3] David A. Muller,[4] Stefan C. Badescu,[1] Vladimir Vasilyev,[1] Jeff L. Brown,[5] Andrew J. Green,[1] and Kelson D. Chabak[1]

AFFILIATIONS

[1] Air Force Research Laboratory, Sensors Directorate, Wright-Patterson AFB, Ohio 45433, USA
[2] Semiconductor Research Center, Wright State University, Dayton, Ohio 45435, USA
[3] Research Laboratory of Electronics, Massachusetts Institute of Technology, Cambridge, Massachusetts 02139, USA
[4] School of Applied and Engineering Physics, Cornell University, Ithaca, New York 14853, USA
[5] KBR, Beavercreek, Ohio 45431, USA

[a] **Author to whom correspondence should be addressed:** hyung_min.jeon.1.ctr@us.af.mil

ABSTRACT

Conductive homoepitaxial Si-doped β-Ga_2O_3 films were fabricated by pulsed laser deposition with an as-deposited 2323 S cm^{-1} conductivity (resistivity = 4.3 × 10^{-4} Ω-cm, carrier concentration = 2.24 × 10^{20} cm^{-3}, mobility = 64.5 cm^2 V^{-1} s^{-1}, and electrical activation efficiency = 77%). High quality homoepitaxial films deposited on commercial (010) Fe-compensated β-Ga_2O substrates were determined by high-resolution transmission electron microscopy and x-ray diffraction. The β-Ga_2O_3 films have ~70% transparency from 3.7 eV (335 nm) to 0.56 eV (2214 nm). The combination of high conductivity and transparency offers promise for numerous ultrawide bandgap electronics and optoelectronic applications.

Transparent conducting oxides (TCOs) have been used in a diverse number of applications, such as displays, flexible electronics, multifunctional windows, and photovoltaics, due to the coexistence of high optical transparency and high electronic conduction.[1] Indium tin oxide (ITO) is a well-known transparent conductor with a low resistivity ρ = 0.37–2 × 10^{-4} Ω-cm (conventional conductivity from 5000 to maximum 27 000 S cm^{-1}).[2] However, ITO is not a viable material as a UV transparent oxide owing to its small bandgap energy (E_g ~ 3.2 eV). Similarly, Al-doped and Ga-doped ZnO have been extensively studied as In-free replacements for ITO with slightly higher bandgaps up to 3.51 eV.[3–10] La-doped $SrSnO_3$ has recently emerged as a candidate wide bandgap TCO material.[11] However, La-doped $SrSnO_3$ film growth has not been developed on native substrates, which may not be suitable for device fabrication, owing to lattice and thermal expansion mismatch. β-Ga_2O_3 is a possible candidate material for UV transparent oxides and high power applications with an energy bandgap of ~4.9 eV.[12] β-Ga_2O_3 has rapidly advanced in a wide array of device applications[13] owing to the wide bandgap,[12] high critical field strength,[14] and native substrate growth.[15] In addition, epitaxial films have been grown with a wide shallow doping range of 10^{15}–10^{20} cm^{-3} fabricated by molecular beam epitaxy (MBE);[16,17] metal organic chemical vapor deposition (MOCVD),[18,19] also known as metal organic vapor phase epitaxy (MOVPE);[20,21] low pressure chemical vapor deposition (LPCVD);[22] halide vapor phase epitaxial (HVPE);[23] and pulsed laser deposition (PLD).[24] However, the conductivity of existing β-Ga_2O_3 films has yet to achieve a high enough level to be suitable as a TCO (at least, ρ ~ 10^{-4} Ω-cm and σ ~ 2000 S cm^{-1}). In order to achieve conductivity in β-Ga_2O_3 films, early reports investigated film growth on diverse substrates. Table I shows that the conductivity of Ga_2O_3 films grown on native substrates, ranging from 6.7 to 1201 S cm^{-1},[17,19,21–25] is much higher than that of films grown on other substrates such as silica 1,[26] $MgAl_2O_4$ 4.76,[27] and Al_2O_3 8.2 S cm^{-1}.[28] Heteroepitaxial films may generate more intrinsic defects that decrease the film conductivity compared to homoepitaxial films due to lattice mismatch between the film and the substrate. In this study, we report on high electrically conducting (2323 S cm^{-1}) Si-doped β-Ga_2O_3 thin films with a bandgap of

TABLE I. Transparent conductive oxide thin films in the recent literature.

References	Conductivity	Films	Substrate	Deposition technique
Najwa[2]	27 000	Sn-doped In_2O_3 (other TCO)	Glass	RF sputtering
Wei[11]	3 000	La-doped $SrSnO_3$ (other TCO)	MgO	PLD
Orita[26]	1	Sn-doped Ga_2O_3 (Ga_2O_3 TCO)	Silica	PLD
Oshima[27]	4.76	Si-doped Ga_2O_3 (Ga_2O_3 TCO)	$MgAl_2O_4$	PLD
Orita[28]	8.2	Sn-doped Ga_2O_3 (Ga_2O_3 TCO)	Al_2O_3	PLD
Feng[19]	6.7	Si-doped Ga_2O_3 (Ga_2O_3 TCO)	Fe:β-Ga_2O_3 (native substrate)	MOCVD
Rafique[22]	13	Si-doped Ga_2O_3 (Ga_2O_3 TCO)	Fe:β-Ga_2O_3 (native substrate)	LPCVD
Leach[23]	189	Si-doped Ga_2O_3 (Ga_2O_3 TCO)	Fe:β-Ga_2O_3 (native substrate)	HVPE
Ahmadi[17]	624	Si-doped Ga_2O_3 (Ga_2O_3 TCO)	Fe:β-Ga_2O_3 (native substrate)	MBE
Baldini[21]	640	Si-doped Ga_2O_3 (Ga_2O_3 TCO)	Fe:β-Ga_2O_3 (native substrate)	MOVPE
Leedy[24]	732	Si-doped Ga_2O_3 (Ga_2O_3 TCO)	Fe:β-Ga_2O_3 (native substrate)	PLD
Lee[25]	1 201	Sn-doped Ga_2O_3 (Ga_2O_3 TCO)	Semi-insulating β-Ga_2O_3 (native substrate)	Mist CVD
This work	2 323	Si-doped Ga_2O_3 (Ga_2O_3 TCO)	Fe:β-Ga_2O_3 (native substrate)	PLD

4.596 eV by pulsed laser deposition on (010) edge-defined film-fed growth substrates.

For sample growth, homoepitaxial Si-doped Ga_2O_3 layers were grown on 5 × 5 mm^2 Fe-doped Ga_2O_3 (010) single crystal substrates (Novel Crystal Technology). A commercial pulsed laser deposition system with a KrF excimer laser was used for PLD deposition with a Ga_2O_3–1 wt. % SiO_2 target. The base pressure of the PLD chamber was 2.66 × 10^{-6} Pa. The 99.99% pure 2-in. diameter ablation target was Ga_2O_3 with 1 wt. % SiO_2 (Plasmaterials, Inc.). The laser energy density of a KrF excimer laser (Coherent COMPexPro 110, λ = 248 nm) was 3 J cm^{-2} with the repetition rate of 10 Hz. The substrate was rotated at 30° s^{-1} and the substrate temperature was between 550 and 590 °C to avoid Fe diffusion into the film from the Fe-doped substrate. Fe diffusion has been observed in an annealing process at 950 °C and involved intrinsic defects in the conductive film.[29] Depositions were performed with different O_2/Ar mixtures at either 8 or 13 Pa.

To determine the film's structural properties, x-ray diffraction (XRD) analysis was performed using a PANalytical X-pert diffractometer with a hybrid monochromator. Surface roughness was observed with a Bruker Dimension Icon atomic force microscope (AFM). Cross-sectional specimens for electron microscopy were prepared using a Helios G4-UX focused ion beam (FIB). Carbon and platinum layers were deposited prior to milling to protect and prevent the sample surface from ion-beam damage. A final milling step of 5 keV was used to further minimize beam damage. High resolution scanning transmission electron microscopy (STEM) was performed with an aberration corrected Titan Themis operated at a beam voltage of 300 keV. Secondary ion mass spectrometry (SIMS) depth profiles were performed for Si and Fe atoms by Eurofins EAG. A Perkin-Elmer Lambda 900 UV/VIS/NIR spectrophotometer was used to measure transmission and absorption over a range of 190–3200 nm (6.52–0.387 eV). Room-temperature Hall-effect measurement was performed using an Accent HL-5500-PC system with a magnetic field strength of 0.5 T. Ohmic contacts of Ti/Al/Ni/Au 20/100/50/50 nm were deposited on the corners of the samples and annealed for 1 min at 470 °C in N_2.

We previously observed that an inherent inhomogeneity of Si dopant in β-Ga_2O_3 films occurred, causing nonuniform current flow, leading to low mobility at high O_2 deposition pressures.[30] In order to further investigate diverse properties of films by changing the PLD plume formation in a higher pressure gas,[31,32] we deposited the films in this work in a series of O_2/Ar mixtures but at higher pressure with respect to reference.[30] Figure 1 shows both the

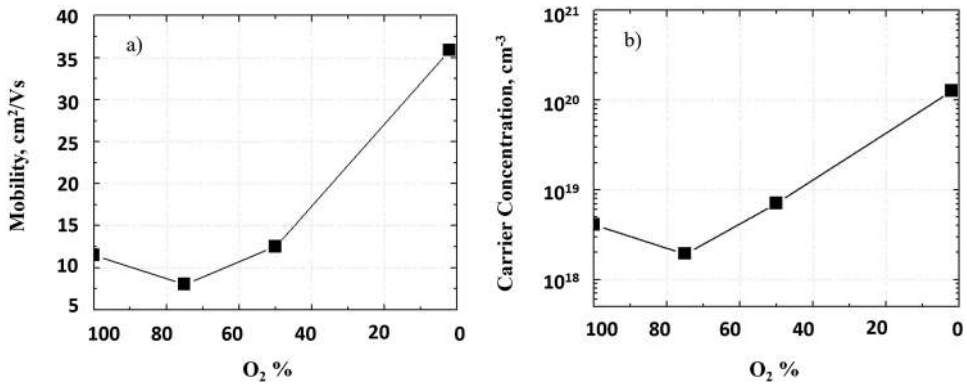

FIG. 1. (a) Hall effect mobility and (b) carrier concentration of Si-doped β-Ga_2O_3 films as a function of O_2% content at a fixed 8 Pa pressure. Remainder of process gas is Ar.

TABLE II. Highly conductive Si-doped β-Ga_2O_3 films with various thickness.

Sample	Thickness (nm)	Doping concentration (cm^{-3})	Mobility ($cm^2\ V^{-1}\ s^{-1}$)
No. 1	40	2.24×10^{20}	64.5
No. 2	41	2.35×10^{20}	53.3
No. 3	152	1.72×10^{20}	54.3
No. 4	241	1.57×10^{20}	60.0
No. 5	512	1.69×10^{20}	56.8

mobility (a) and carrier concentration (b) increase as a function of oxygen content during deposition. The residual gas species is Ar. The samples were deposited under 100%, 75%, 50%, and 2% oxygen at a fixed 8 Pa. Both carrier concentration and mobility show general improvement in lower oxygen content depositions. Regarding higher conductivity at lower oxygen deposition pressure, the experimental results are in agreement with those of Müller *et al.*[33] and Leedy *et al.*[30] For highly conductive oxide film deposition in pure Ar gas, it has already been observed in polycrystalline Ga-doped ZnO grown by PLD.[34] For β-Ga_2O_3 PLD deposition, the oxygen from the polycrystalline Ga_2O_3 PLD target may be sufficient for growing the film such that additional oxygen process gas yields films with higher resistivity. Accordingly, high quality films with enhanced 44.3 $cm^2\ V^{-1}\ s^{-1}$ mobility and high carrier concentration ($1.941 \times 10^{20}\ cm^{-3}$) were deposited in pure Ar at 8 Pa. Similarly, films in much higher (Ar 13 Pa) gas pressure are deposited and observed in Table II to have higher (~60 $cm^2\ V^{-1}\ s^{-1}$) mobilities than films (44.3 $cm^2\ V^{-1}\ s^{-1}$ mobility) in 8 Pa of Ar. For the Si dopant in β-Ga_2O_3, the mean free path between the collisions of Si, Ga, and O is shortened with increasing pressure in the PLD chamber. The shortened mean free path increases the molecular number density that enables Si to dope in β-Ga_2O_3. The uniform Si dopant in β-Ga_2O_3 increases the electrical activation efficiency, leading to the improved conductivity.

Representative selected samples were deposited with thicknesses from 40 to 512 nm (as shown in Table II, the growth rate is about 96 nm/h) in order to demonstrate the repeatability of film quality, electrical activation efficiency with different thicknesses, and optical properties of thicker films. The average electrical properties of the five films from thinnest (40 nm) to thickest (512 nm) achieved a room temperature carrier concentration of $\sim 1.9 \times 10^{20}\ cm^{-3}$ and mobility of ~57.7 $cm^2\ V^{-1}\ s^{-1}$. The samples were also characterized via temperature-dependent Hall effect measurement, where the temperature was changed from 10 to 290 K. For sample No. 1 (highest conductivity), the measured room temperature (290 K) electron mobility was 64.5 $cm^2\ V^{-1}\ s^{-1}$ and the maximum mobility of 82 $cm^2\ V^{-1}\ s^{-1}$ occurred at the lowest temperature, as shown in Fig. 2(b). The carrier concentration remained nearly constant at $2.24 \times 10^{20}\ cm^{-3}$ over the whole temperature range. The calculated conductivity at room temperature using the carrier concentration of $2.24 \times 10^{20}\ cm^{-3}$ and mobility of 64.5 $cm^2\ V^{-1}\ s^{-1}$ is 2323 S cm^{-1} (4.3×10^{-4} Ω-cm resistivity), which represents the highest conductivity for the epitaxial β-Ga_2O_3 films.

To support the electrical properties, secondary ion mass spectrometry (SIMS) depth profiles were performed. SIMS of Si and Fe in the thinnest (sample No. 1, 40 nm) and thickest (sample No. 5, 512 nm) films is presented in Fig. 3. In neither case is the conductivity significantly affected by diffusion of these elements into the interface region. In particular, the Fe concentration in both films is about $10^{18}\ cm^{-3}$, far below the Si concentration of about $3.0 \times 10^{20}\ cm^{-3}$. The Si and Fe concentrations can be compared with the donor N_D and acceptor N_A concentrations, respectively, calculated from the temperature-dependent Hall effect measurements.[35,36] For sample No. 1, $N_D = 3.44 \times 10^{20}$ and $N_A = 1.13 \times 10^{20}\ cm^{-3}$, and for sample No. 5, $N_D = 2.84 \times 10^{20}$ and $N_A = 1.15 \times 10^{20}\ cm^{-3}$. The Hall effect values of N_D are very close to the SIMS values of [Si], showing the accuracy of the calculations. In addition, note that $N_A \gg$ [Fe], showing that Fe is not a dominant acceptor in any case, and the same is probably true for any other background impurity. The dominant acceptors are likely isolated Ga vacancies V_{Ga} or Si_{Ga}–V_{Ga}

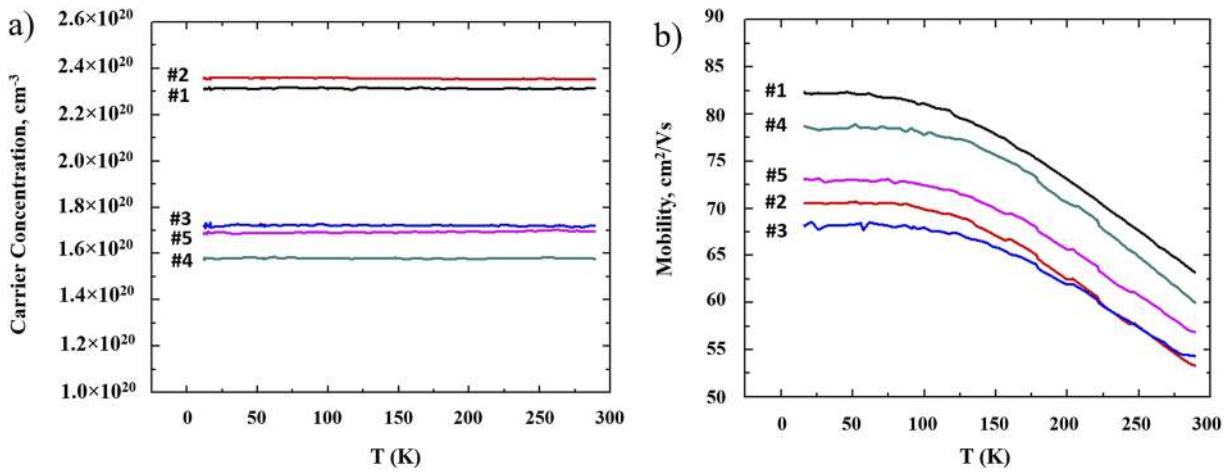

FIG. 2. (a) Carrier concentration and (b) mobility of Si-doped β-Ga_2O_3 films from temperature-dependent Hall effect measurement (sample No. 1, No. 2, No. 3, No. 4, and No. 5).

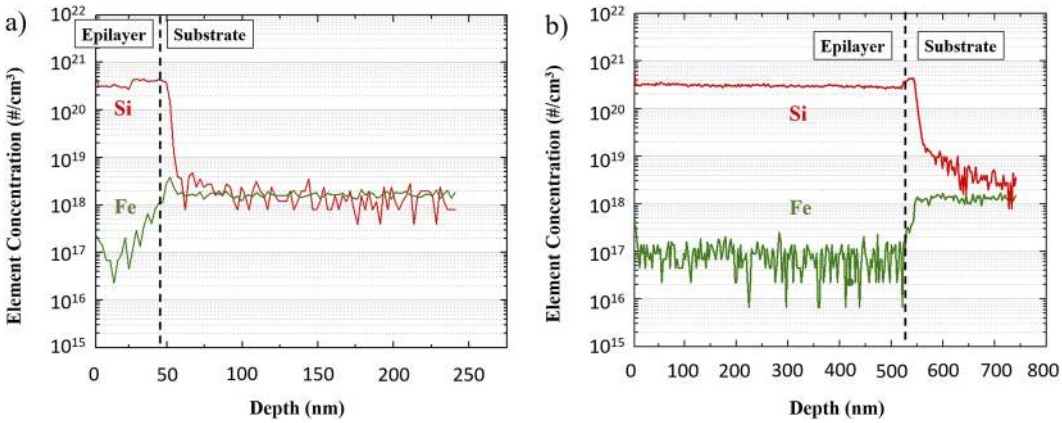

FIG. 3. SIMS depth profile of Si and Fe in (a) 40 nm and (b) 512 nm thickness of Si-doped Ga_2O_3 films on the Fe-doped Ga_2O_3 [010] substrate.

complexes. Such a scenario, in which the dopant participates in acceptor complexes, holds for many highly doped semiconductors, e.g., Ga-doped ZnO.[36] The electrical activation efficiencies, defined as $(N_D-N_A)/[Si]$, for sample No. 1 (40 nm thickness) and sample No. 5 (512 nm thickness) are 77% and 56%, respectively.

X-ray diffraction $\theta/2\theta$ and rocking curve (RC) ω scans were performed to study the crystal quality and strain of the films. Overall, the film peaks are sharp and overlap the substrate peak, indicating high quality epitaxy. Figures 4(a) and 4(b) show that a slight right shoulder is observed in the $\theta/2\theta$ scan. It indicates that the Si-doped β-Ga_2O_3 film has a slight in-plane [010] tensile strain and compressed along the [010] direction (~0.07° 2θ shift). This strain can primarily be attributed to the smaller Si (IV) ion dopant substituting the bigger Ga (III) ion in the film in addition to other potential factors, including thermal influences and defects from the growth. In the subsequent ω RC scan on β-Ga_2O_3 [020], a full width half maximum (FWHM) in Fig. 4(d) shows 46.8 arc sec, averaged over several samples (from 41 to 512 nm thickness), from the film (Si-doped β-Ga_2O_3) compared to the substrate (Fe-doped β-Ga_2O_3), which has 32.4 arc sec FWHM, as shown in Fig. 4(c). Thus, the epitaxial film structure is consistent with the substrate. The slight right shoulder from the film RC also supports the evidence of slight tensile strain in the Si-doped β-Ga_2O_3 film (~0.02° shift) in comparison with the substrate.

Atomic force microscopy (AFM) in a 1 × 1 μm^2 area was performed to investigate the surface morphology. The overall surface image in Fig. 5 shows surface morphologies that reveal smooth film surfaces with a root-mean-square roughness (RMS) of ~0.4 nm, slightly rougher than the measured ~0.1 nm RMS roughness from the bare substrate.

To further investigate the structural properties, high-resolution STEM was performed. We examined the film by a high-angle annular dark field (HAADF) STEM to confirm the film quality and the film thickness, as shown in Fig. 6. The thickness of the film was determined by the presence of the interface between the film and the substrate that shows a bright contrast, likely originating from

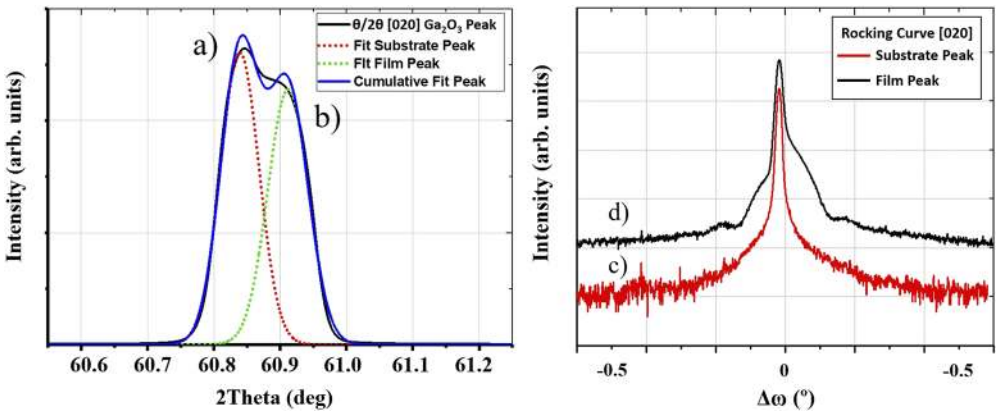

FIG. 4. Symmetrical $\theta/2\theta$ scan is for the (a) Fe-doped β-Ga_2O_3 substrate and (b) Si-doped β-Ga_2O_3 film. XRD rocking curve on β-Ga_2O_3 [020] of the (c) Fe-doped β-Ga_2O_3 substrate and (d) Si-doped β-Ga_2O_3 film.

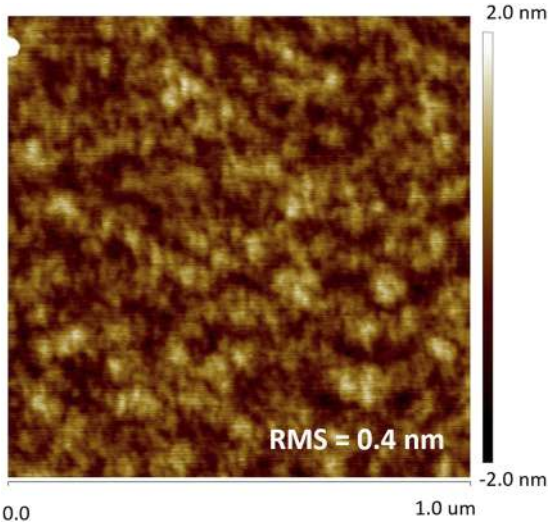

FIG. 5. 1 × 1 μm^2 atomic force microscopy (AFM) image of the surface of the Si-doped β-Ga_2O_3 film.

point defects, as shown in Fig. 6(a). The film thickness was measured to be 40 nm, consistent with that obtained from step height profilometry and SIMS. The film was grown uniformly in the β-phase except for a very thin (<1 nm) surface layer of γ-Ga_2O_3 [110]. The formation of a γ-Ga_2O_3 surface layer has also been observed in β-Ga_2O_3 films grown by conventional MBE[37] and S-MBE,[38] suggesting that this is likely to be an intrinsic growth mechanism occurring in homoepitaxial β-Ga_2O_3 [010] growths.

Reflectance (R_m) and transmittance (T_m) measurements were performed on sample No. 5 (Si-doped β-Ga_2O_3, 512-nm thick, grown on double-side-polished Fe-doped β-Ga_2O_3 [010]) over a range of 190–3200 nm (6.52–0.387 eV). Curves of R_m and T_m, along with absorbance $A_m = 1 - R_m - T_m$, are plotted in Fig. 7(a). The optical transmittance is ~70% from 3.7 eV (335 nm) to 0.56 eV (2214 nm). In the deep ultraviolet (DUV) region, the transmission was reduced, e.g., to 20% at 4.42 eV (280 nm). The bandgap can be calculated from a linear plot of α^2 vs energy E, as shown in Fig. 7(b). The absorption coefficient α is determined from an exact formula that holds for small α as well as large α.[39] (Note that the usual Tauc plot of $(\alpha E)^2$ vs E is correct only for amorphous materials.) Band filling causes the bandgap (4.596 eV) of this highly conductive layer to be larger than that of the nonconductive substrate by the so-called Moss–Burstein (MB) shift, about 0.32 eV for the concentration of sample No. 5 listed in Table II.

To investigate the influence of the substrate on the optical properties, we distinguish between the thin film layer with the substrate and the substrate alone. The differences in the optical properties of the Si-doped β-Ga_2O_3 layer and the Fe-doped β-Ga_2O_3 substrate are best illustrated by a comparison of their absorption (alpha) and reflection (R) coefficients, calculated from the reflectance and transmittance and shown in Fig. 8. The big difference in R is the prominent plasmonic reflectance beginning at about 0.57 eV in the layer, and a difference in alpha is the free-carrier absorption below about 1 eV. Both of these effects are due to the free carriers generated by the Si donors. Another difference in absorption occurs from 2 to 3 eV and is possibly due to Si_Ga–V_Ga acceptors in the Si-doped layer. In short, the most prominent features seen in the layer but not the substrate are the absorptions from 0.4 to 1.0 eV and 2.0 to 3.5 eV, and the reflective feature is below 0.57 eV.

Figure 9 shows the overall trend of mobility vs carrier concentration of β-Ga_2O_3 films using different deposition techniques and dopants.[46–52] In highly degenerate semiconductors, the mobility decreases in the high concentration range mainly due to the Si_{Ga} donors, V_{Ga} acceptors, and Si_{Ga}–V_{Ga} complex acceptors, as explained below. In fact, the key method of increasing both concentration and mobility is to decrease the acceptor

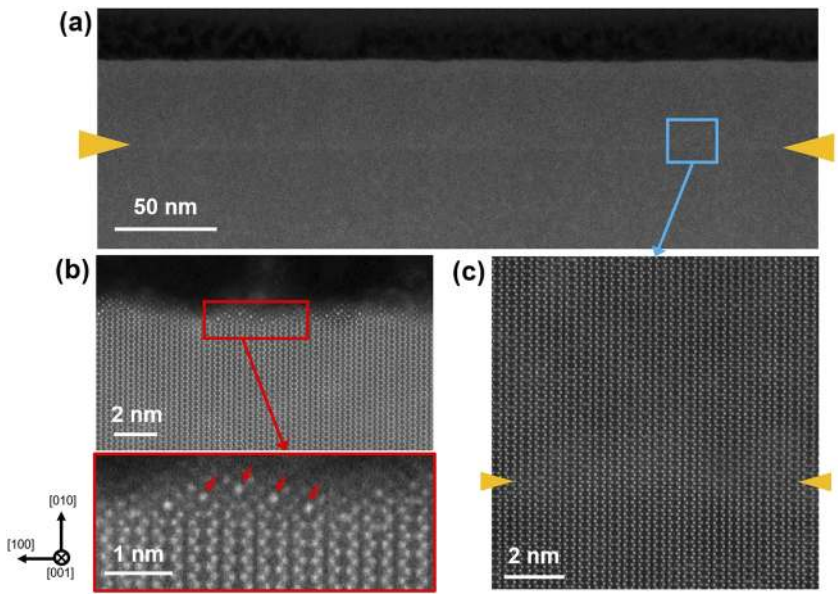

FIG. 6. HAADF-STEM images of the β-Ga_2O_3 film grown by PLD on the Fe-doped β-Ga_2O_3 substrate. (a) Overview of the sample at low magnification shows the interface between the PLD–grown film and the substrate. The interface is marked with orange arrows. (b) The film is grown uniformly in the β-phase (001) except at the surface where 1–2 monolayers of the γ-phase are formed. The enlarged image from the surface region shows the γ-phase (110) crystal structure. (c) Enlarged area from (a) at the interface shows the uniform β-phase without any large-scale defects or dislocations, confirming a smooth transition from the substrate to the film.

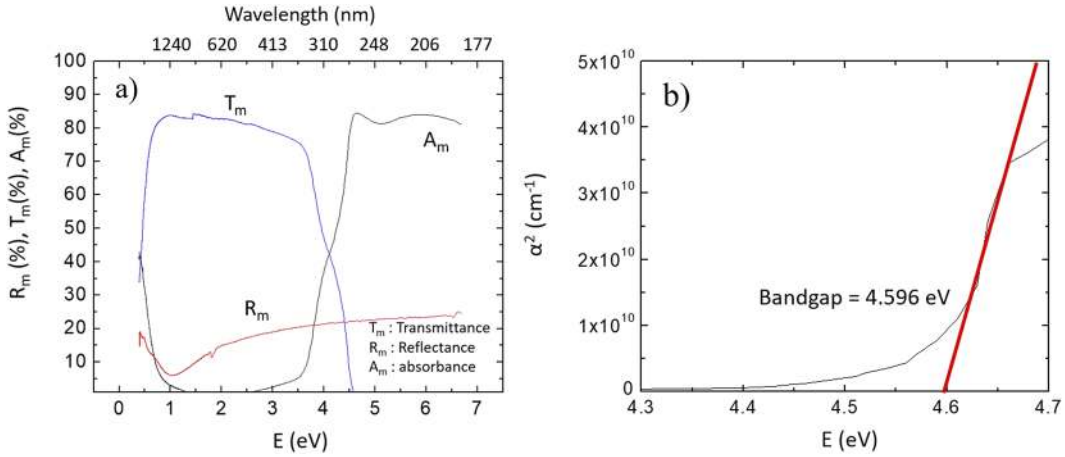

FIG. 7. (a) Transmittance, reflectance, and absorbance of 512 nm thick Si-doped β-Ga_2O_3 [010] and (b) measured bandgap energy of Si-doped β-Ga_2O_3 [010].

concentration. We have earlier developed an expression for mobility[35] as a function of the compensation ratio K = N_A/N_D. For the five samples in Table II, K is 0.328, 0.393, 0.430, 0.378, and 0.405. If all the acceptors in each sample could be eliminated or passivated, i.e., K = 0, the mobilities would be 105, 92, 104, 103, and 103 cm^2 V^{-1} s^{-1}, respectively. Moreover, the conductivities would be more than double; e.g., for sample No. 1, it would increase from 2323 to 7516 S cm^{-1}. This calculation shows the enormous benefit of decreasing N_A. In earlier literature shown in Fig. 9, a mobility of 15 cm^2 V^{-1} s^{-1} was achieved at 5 × 10^{20} cm^{-3},[25] 26.5 cm^2 V^{-1} s^{-1} at 1.74 × 10^{20} cm^{-3},[24] and 30 cm^2 V^{-1} s^{-1} at 1.37 × 10^{20} cm^{-3}.[30] However, our films have higher mobilities, likely due to lower values of K. Of course, other scattering mechanisms may also be responsible for lower mobilities.[40]

To understand the nature of defect complexes and their contribution to mobility improvement in the absence of dislocations or grain boundaries, we performed first principles calculations of formation energies. The large Si concentrations in the experiment correspond to one Si atom per 100–200 Ga atoms, which is the size of typical supercell calculations. This means that Si donors and thermodynamically driven gallium vacancies coexist in close proximity. We performed first principles modeling to find formation energies and electronic structures of silicon-gallium vacancy defect complexes. We used the projector augmented wave function[41] pseudopotential method implemented in the Vienna *Ab Initio* Simulation Package[42] with an energy cutoff of 400 eV. For structural optimizations, we used the revised Perdew–Burke–Ernzerhof functional for solid (PBESol),[43] followed by single point total energy calculations with the hybrid Heyd–Scuseria–Ernzerhof (HSE).[44] For the latter, we used a Hartree–Fock mixing parameter of 0.305. The supercell model corresponded to eight crystallographic unit cells (160 atoms) and used a 2 × 2 × 2 k-point grid. The formation energy E_f depends strongly on the growth conditions, i.e., gallium-rich vs oxygen-rich. Different growth conditions determine different values of gallium chemical potential μ_{Ga}, which enters into the expression of formation energy $E_f(D) = E(D) - E(bulk) - \sum_{Ga} n_{Ga}\mu_{Ga} - \sum_{Si} n_{Si}\mu_{Si} + qE_F + E_{Corr}$,[45] where D stands for the supercell with a defect state, E_F stands for the Fermi level relative to the top of the

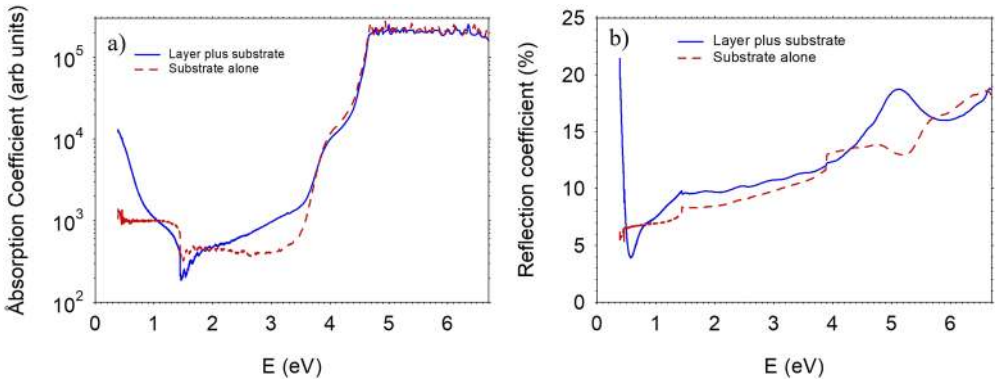

FIG. 8. (a) Absorption coefficient of the 512 nm thick Si-doped β-Ga_2O_3 film with the substrate (Fe-doped β-Ga_2O_3) vs bare substrate alone (Fe-doped β-Ga_2O_3). (b) Reflection coefficient of the 512 nm thick Si-doped β-Ga_2O_3 film with the substrate (Fe-doped β-Ga_2O_3) vs bare substrate alone (Fe-doped β-Ga_2O_3).

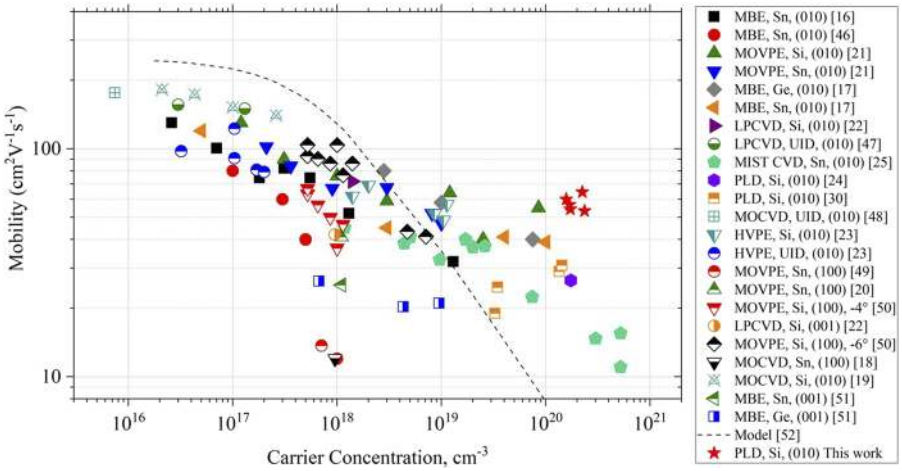

FIG. 9. Mobility vs carrier concentration of n-type-doped homoepitaxial β-Ga_2O_3 films in the recent literature.

valence band in the unperturbed (*bulk*) lattice, and E_{Corr} stands for the sum of several finite size corrections: band alignment, charge image, and band filling corrections. Here, n_{Si} is the number of added silicon atoms and $n_{Ga} = -n_{Si} - 1$ is the number of added gallium atoms (including the vacancies). For Ga-rich conditions, $\mu_{Ga,Max} = -3.71$ eV, corresponding to the metallic gallium phase, whereas for O_2-rich conditions, $\mu_{Ga,min} = -10.74$ eV.[46–52] The large magnitude of the latter determines a large shift downward of E_f as the number of Si substitutional atoms increases (increasing the number of removed Ga atoms). For Ga-rich conditions, the defect complexes $D(n_{Si}) = n_{Si}Si - V_{Ga}$ have formation energies comparable to that of a single vacancy V_{Ga}, i.e., between −1 and −0.4 eV for $E_F = E_{gap}$ (i.e., the Fermi level at the bottom of the conduction band CBM). By increasing n_{Si}, the charges of these defects decrease by 1: from V_{Ga}^{-3} of gallium vacancy to $Si - V_{Ga}^{-2}$, $2Si - V_{Ga}^{-1}$, and $3Si - V_{Ga}^{0}$. These are deep acceptors with energy levels situated at 2.8 eV below the conduction band (by comparison, the gallium vacancy has a defect level at 1.2 eV below the conduction band). The situation is dramatically changed for O_2-rich conditions when the complexes $D(n_{Si})$ with $n_{Si} > 0$ become energetically favorable: $E_{f,O_2-rich}(Si - V_{Ga}^{-2}) = -8.23$ eV, $E_{f,O_2-rich}(2Si - V_{Ga}^{-1}) = -17.74$ eV, and $E_{f,O_2-rich}(3Si - V_{Ga}^{0}) = -25.77$ eV (for $E_F = E\_gap$). The lower charge states of these defects reduce significantly the charge impurity scattering. The actual experimental growth conditions lay in the range between Ga-rich and O_2-rich, closer to the latter.

In conclusion, transparent conducting oxide (TCO) thin films of Si-doped β-Ga_2O_3 by PLD were investigated by XRD, AFM, TEM, SIMS, Hall effect, and UV spectrophotometer. The highest conductivity achieved was 2323 cm^{-1} with 64.5 cm^2 V^{-1} s^{-1} mobility and 2.24×10^{20} cm^{-3} carrier concentration. The calculated donor N_D value of 3.44×10^{20} cm^{-3} is very similar to the Si chemical concentration of about 3×10^{20} cm^{-3} from SIMS, which achieved 77% electrical activation efficiency. The bandgap energy of the highly conductive Si-doped β-Ga_2O_3 film was 4.596 eV. These results indicate that Si impurities are uniformly doped in β-Ga_2O_3 with low level structural distortion, and this TCO achieves transmission into the UV region, which opens up the potential for optoelectronic applications.

This research was performed while H. M. Jeon held an NRC Research Associateship award at the Air Force Research Laboratory. The microscopy was supported by the Cornell/AFOSR ACCESS center of excellence (Grant No. FA955018-1-0529). This work made use of the Cornell Center for Materials Research (CCMR) Shared Facilities, which are supported through the NSF MRSEC Program (Grant No. DMR-1719875). The FEI Titan Themis 300 was acquired under Grant No. NSF-MRI-1429155, with additional support from Cornell University, the Weill Institute, and the Kavli Institute at Cornell.

D.C.L. acknowledges support from AFOSR, Grant No. FA9550-RY18COR800; AFRL, Contract No. FA8075-14-D-0025; and NSF, Grant No. DMR-1800139. We wish to thank T. A. Cooper, W. Rice, and D. McFarland for critical technical support in these experiments. The first principles modeling was performed through the High Performance Computing program of the DoD, using the AFR and Navy DSRCs.

AUTHOR DECLARATIONS

Conflict of Interest

The authors have no conflicts to disclose.

DATA AVAILABILITY

The data that support the findings of this study are available from the corresponding author upon reasonable request.

REFERENCES

[1] David S. Ginley, *Handbook of Transparent Conductors* (Springer, 2010). Photovoltaics & Electronic Materials, Center & Basic Sciences Ctr. NRELGoldenUSA, https://link.springer.com/book/10.1007/978-1-4419-1638-9#editorsandaffiliations.

[2] S. Najwa, A. Shuhaimi, N. A. Talik, N. Ameera, M. Sobri, and M. Rusop, Appl. Surf. Sci. **479**, 1220 (2019).

[3] H. S. Das, R. Das, P. K. Nandi, S. Biring, and S. K. Maity, Appl. Phys. A **127**, 225 (2021).

[4] B. Bayraktaroglu, K. Leedy, and R. Bedford, Appl. Phys. Lett. **93**, 022104 (2008).

[5] G. Fang, D. Li, and B.-L. Yao, Vacuum **68**, 363 (2002).

[6]T. Minami, S. Suzuki, and T. Miyata, Thin Solid Films **398-399**, 53 (2001).
[7]H. Tanaka, K. Ihara, T. Miyata, H. Sato, and T. Minami, J. Vac. Sci. Technol. A **22**, 1757 (2004).
[8]H. Agura, A. Suzuki, T. Matsushita, T. Aoki, and M. Okuda, Thin Solid Films **445**, 263 (2003).
[9]S.-M. Park, T. Ikegami, K. Ebihara, and P.-K. Shin, Appl. Surf. Sci. **253**, 1522 (2006).
[10]T. Minami, S. Ida, and T. Miyata, Thin Solid Films **416**, 92 (2002).
[11]M. Wei, A. V. Sanchela, B. Feng, Y. Ikuhara, H. J. Cho, and H. Ohta, Appl. Phys. Lett. **116**, 022103 (2020).
[12]Z. Galazka, R. Uecker, K. Irmscher, M. Albrecht, D. Klimm, M. Pietsch, M. Brützam, R. Bertram, S. Ganschow, and R. Fornari, Cryst. Res. Technol. **45**, 1229 (2010).
[13]G. Jessen, K. Chabak, A. Green, N. Moser, J. McCandless, K. Leedy, A. Crespo, and S. Tetlak, in *2017 IEEE Compound Semiconductor Integrated Circuit Symposium (CSICS)* (IEEE, 2017), pp. 1–4.
[14]A. J. Green, K. D. Chabak, E. R. Heller, R. C. Fitch, M. Baldini, A. Fiedler, K. Irmscher, G. Wagner, Z. Galazka, S. E. Tetlak, A. Crespo, K. Leedy, and G. H. Jessen, IEEE Electron Device Lett. **37**, 902 (2016).
[15]K. Irmscher, Z. Galazka, M. Pietsch, R. Uecker, and R. Fornari, J. Appl. Phys. **110**, 063720 (2011).
[16]K. Sasaki, A. Kuramata, T. Masui, E. G. Víllora, K. Shimamura, and S. Yamakoshi, Appl. Phys. Express **5**, 035502 (2012).
[17]E. Ahmadi, O. S. Koksaldi, X. Zheng, T. Mates, Y. Oshima, U. K. Mishra, and J. S. Speck, Appl. Phys. Express **10**, 071102 (2017).
[18]X. Du, Z. Li, C. Luan, W. Wang, M. Wang, X. Feng, H. Xiao, and J. Ma, J. Mater. Sci. **50**, 3252 (2015).
[19]Z. Feng, A. F. M. Anhar Uddin Bhuiyan, M. R. Karim, and H. Zhao, Appl. Phys. Lett. **114**, 250601 (2019).
[20]M. Baldini, M. Albrecht, A. Fiedler, K. Irmscher, D. Klimm, R. Schewski, and G. Wagner, J. Mater. Sci. **51**, 3650 (2016).
[21]M. Baldini, M. Albrecht, A. Fiedler, K. Irmscher, R. Schewski, and G. Wagner, ECS J. Solid State Sci. Technol. **6**, Q3040 (2017).
[22]S. Rafique, M. R. Karim, J. M. Johnson, J. Hwang, and H. Zhao, Appl. Phys. Lett. **112**, 052104 (2018).
[23]J. H. Leach, K. Udwary, J. Rumsey, G. Dodson, H. Splawn, and K. R. Evans, APL Mater. **7**, 022504 (2019).
[24]K. D. Leedy, K. D. Chabak, V. Vasilyev, D. C. Look, J. J. Boeckl, J. L. Brown, S. E. Tetlak, A. J. Green, N. A. Moser, A. Crespo, D. B. Thomson, R. C. Fitch, J. P. McCandless, and G. H. Jessen, Appl. Phys. Lett. **111**, 012103 (2017).
[25]S.-d. Lee, K. Kaneko, and S. Fujita, Jpn. J. Appl. Phys., Part 1 **55**, 1202B8 (2016).
[26]M. Orita, H. Ohta, M. Hirano, and H. Hosono, Appl. Phys. Lett. **77**, 4166 (2000).
[27]T. Oshima, K. Matsuyama, K. Yoshimatsu, and A. Ohtomo, J. Cryst. Growth **421**, 23 (2015).
[28]M. Orita, H. Hiramatsu, H. Ohta, M. Hirano, and H. Hosono, Thin Solid Films **411**, 134 (2002).
[29]M. H. Wong, K. Sasaki, A. Kuramata, S. Yamakoshi, and M. Higashiwaki, Appl. Phys. Lett. **106**, 032105 (2015).
[30]K. D. Leedy, K. D. Chabak, V. Vasilyev, D. C. Look, K. Mahalingam, J. L. Brown, A. J. Green, C. T. Bowers, A. Crespo, D. B. Thomson, and G. H. Jessen, APL Mater. **6**, 101102 (2018).
[31]X. Y. Chen, S. B. Xiong, Z. S. Sha, and Z. G. Liu, Appl. Surf. Sci. **115**, 279 (1997).
[32]A. Ojeda-G-P, M. Döbeli, and T. Lippert, Adv. Mater. Interfaces **5**, 1701062 (2018).
[33]S. Müller, H. Von Wenckstern, D. Splith, F. Schmidt, and M. Grundmann, Phys. Status Solidi A **211**, 34 (2014).
[34]R. C. Scott, K. D. Leedy, B. Bayraktaroglu, D. C. Look, and Y.-H. Zhang, Appl. Phys. Lett. **97**, 072113 (2010).
[35]D. C. Look and K. D. Leedy, Sci. Rep. **9**, 1290 (2019).
[36]D. C. Look, K. D. Leedy, L. Vines, B. G. Svensson, A. Zubiaga, F. Tuomisto, D. R. Doutt, and L. J. Brillson, Phys. Rev. B **84**, 115202 (2011).
[37]C. S. Chang, N. Tanen, V. Protasenko, T. J. Asel, S. Mou, H. G. Xing, D. Jena, and D. A. Muller, APL Mater. **9**, 051119 (2021).
[38]P. Vogt, F. V. E. Hensling, K. Azizie, C. S. Chang, D. Turner, J. Park, J. P. McCandless, H. Paik, B. J. Bocklund, G. Hoffman, O. Bierwagen, D. Jena, H. G. Xing, S. Mou, D. A. Muller, S.-L. Shang, Z.-K. Liu, and D. G. Schlom, APL Mater. **9**, 031101 (2021).
[39]D. C. Look, B. Wang, and K. D. Leedy, Opt. Eng. **56**, 034112 (2017).
[40]Y. Kang, K. Krishnaswamy, H. Peelaers, and C. G. Van De Walle, J. Phys.: Condens. Matter **29**, 234001 (2017).
[41]G. Kresse and D. Joubert, Phys. Rev. B **59**, 1758 (1999).
[42]J. Heyd, G. E. Scuseria, and M. Ernzerhof, J. Chem. Phys. **118**, 8207 (2003).
[43]J. P. Perdew, A. Ruzsinszky, G. I. Csonka, O. A. Vydrov, G. E. Scuseria, L. A. Constantin, X. Zhou, and K. Burke, Phys. Rev. Lett. **100**, 136406 (2009).
[44]G. Kresse and J. Hafner, Phys. Rev. B **49**, 14251 (1994).
[45]C. Freysoldt, B. Grabowski, T. Hickel, J. Neugebauer, G. Kresse, A. Janotti, and C. G. Van De Walle, Rev. Mod. Phys. **86**, 253 (2014).
[46]H. Okumura, M. Kita, K. Sasaki, A. Kuramata, M. Higashiwaki, and J. S. Speck, Appl. Phys. Express **7**, 095501 (2014).
[47]Y. Zhang, Z. Feng, M. R. Karim, and H. Zhao, J. Vac. Sci. Technol. A **38**, 050806 (2020).
[48]Y. Zhang, F. Alema, A. Mauze, O. S. Koksaldi, R. Miller, A. Osinsky, and J. S. Speck, APL Mater. **7**, 022506 (2019).
[49]D. Gogova, M. Schmidbauer, and A. Kwasniewski, CrystEngComm **17**, 6744 (2015).
[50]M. Baldini, Z. Galazka, and G. Wagner, Mater. Sci. Semicond. Process. **78**, 132 (2018).
[51]S.-H. Han, A. Mauze, E. Ahmadi, T. Mates, Y. Oshima, and J. S. Speck, Semicond. Sci. Technol. **33**, 045001 (2018).
[52]N. Ma, N. Tanen, A. Verma, Z. Guo, T. Luo, H. (Grace) Xing, and D. Jena, Appl. Phys. Lett. **109**, 212101 (2016).